BIOCHEMISTRY
including biophysical chemistry & molecular biology

Article

pubs.acs.org/biochemistry

Cyclic Nucleotide-Gated Channel Subunit Glycosylation Regulates Matrix Metalloproteinase-Dependent Changes in Channel Gating

Starla E. Meighan,[†] Peter C. Meighan,[†] Elizabeth D. Rich,[†] R. Lane Brown,[‡] and Michael D. Varnum*[,§]

[†]Program in Neuroscience, Department of Integrative Physiology and Neuroscience, [‡]WWAMI Medical Education Program, and [§]Center for Integrated Biotechnology, Washington State University, P.O. Box 647620, Pullman, Washington 99164, United States

ABSTRACT: Cyclic-nucleotide gated (CNG) channels are essential for phototransduction within retinal photoreceptors. We have demonstrated previously that the enzymatic activity of matrix metalloproteinase-2 and -9, members of the matrix metalloproteinase (MMP) family of extracellular, Ca^{2+}- and Zn^{2+}-dependent proteases, enhances the ligand sensitivity of both rod (CNGA1 and CNGB1) and cone (CNGA3 and CNGB3) CNG channels. Additionally, we have observed a decrease in the maximal CNG channel current (I_{max}) that begins late during MMP-directed gating changes. Here we demonstrate that CNG channels become nonconductive after prolonged MMP exposure. Concurrent with the loss of conductive channels is the increased relative contribution of channels exhibiting nonmodified gating properties, suggesting the presence of a subpopulation of channels that are protected from MMP-induced gating effects. CNGA subunits are known to possess one extracellular core glycosylation site, located at one of two possible positions within the turret loop near the pore-forming region. Our results indicate that CNGA glycosylation can impede MMP-dependent modification of CNG channels. Furthermore, the relative position of the glycosylation site within the pore turret influences the extent of MMP-dependent proteolysis. Glycosylation at the site found in CNGA3 subunits was found to be protective, while glycosylation at the bovine CNGA1 site was not. Relocating the glycosylation site in CNGA1 to the position found in CNGA3 recapitulated CNGA3-like protection from MMP-dependent processing. Taken together, these data indicate that CNGA glycosylation may protect CNG channels from MMP-dependent proteolysis, consistent with MMP modification of channel function having a requirement for physical access to the extracellular face of the channel.

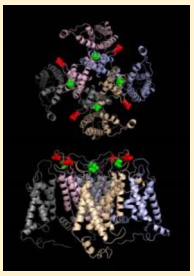

Cyclic nucleotide-gated (CNG) channels are members of the voltage-gated channel superfamily and are activated by the intracellular binding of cyclic nucleotides. In the visual system, CNG channels are the principal ion channels responsible for transduction of a light-induced decrease in the level of intracellular cGMP into a photoreceptor electrical response. Native photoreceptor CNG channels are heterotetrameric proteins composed of two structurally related subunit types: CNGA1 and CNGB1 in rod photoreceptors and CNGA3 and CNGB3 in cone photoreceptors.[1,2] The sensitivity of CNG channels to their endogenous ligands, cGMP and cAMP, is regulated by various intracellular effectors,[3] including calcium sensor proteins,[4,5] serine/threonine and tyrosine kinases,[6−8] and phosphoinositides.[9−12] The altered channel gating properties produced by these regulatory inputs are thought to contribute to light−dark adaptation[3,13] and paracrine and circadian control of photoreceptor sensitivity.[14,15]

We have recently demonstrated that CNG channel function can be influenced by members of a family of secreted endopeptidases, matrix metalloproteinases (MMPs), via proteolytic modification of CNGA subunits.[16] For both heterologously expressed and native CNG channels, extracellular exposure to MMPs dramatically increased the apparent affinity for cGMP and the efficacy of cAMP. The gating changes with MMPs occurred more rapidly when the channels were mostly closed compared to channels held open in a saturating concentration of cGMP, suggesting state-dependent exposure of critical extracellular regions. These findings highlighted potential extracellular control of channel ligand sensitivity. Given that MMP modifications profoundly alter the ligand sensitivity of CNG channels, we predicted that other extracellular features might regulate processing of channels by MMPs. CNGA subunits typically possess a single, extracellular glycosylation site within the pore turret loop. Glycosylation is well-characterized as a critical factor for maturation, trafficking, and stability of membrane proteins[17−20] and can also influence protein activity.[21,22] However, it has been demonstrated previously that the absence of CNGA pore turret glycosylation has no apparent effect on the functional expression or gating properties of CNG channels.[23,24] Thus, the functional importance of CNGA subunit glycosylation has remained elusive.

We hypothesized that CNGA pore turret glycosylation decreases susceptibility to extracellular subunit proteolysis, providing protection from MMP-dependent gating changes. Here we demonstrate that a subpopulation of channels composed of CNGA subunits, with or without CNGB subunits, is protected from MMP-dependent proteolysis. Protection from MMP-mediated processing was observed for both heterologously expressed and native retinal CNG channels. We show that channel protection is primarily due to glycosylation in the CNGA pore turret and is dependent on the location of the glycosylation site within the turret. These findings suggest that

Received: June 25, 2013
Revised: October 23, 2013
Published: October 28, 2013

the conserved CNG channel pore turret glycosylation modulates MMP-dependent regulation of CNG channel gating.

EXPERIMENTAL PROCEDURES

Molecular Biology and Functional Expression. For heterologous expression in *Xenopus laevis* oocytes, the coding sequence for human CNGA3[25] was engineered to have an amino-terminal 3X-FLAG epitope tag.[26] The human CNGB3 clone was isolated previously from human retinal cDNA.[27] FLAG-tagged bovine CNGA1 was generated as previously described.[26] HA-tagged human CNGB1 was a generous gift from S. E. Gordon. All channel cDNAs were subcloned previously into pGEMHE. Site-directed mutagenesis of CNGA3 and CNGA1 was conducted as previously described.[27] Oocytes were isolated and microinjected with ~5 ng of mRNA (for all constructs). For efficient generation of heteromeric channels, the ratio of CNGA mRNA to CNGB mRNA was 1:2.5.[26] Oocytes were incubated in ND96 [96 mM NaCl, 2 mM KCl, 1.8 mM $CaCl_2$, 1 mM $MgCl_2$, and 5 mM HEPES (pH 7.6) supplemented with 10 μg/mL gentamycin] at 17−19 °C.

Electrophysiology. One to seven days after microinjection of mRNA, patch-clamp experiments were performed in the inside-out configuration. Recordings were taken at 20−23 °C. Voltage control was provided by an Axopatch 200B amplifier (Molecular Devices, Sunnyvale, CA; formerly Axon Instruments); macroscopic current data were acquired using Pulse (HEKA Elektronik, Lambrecht, Germany) with a sampling frequency of 25 kHz, low-pass filtered at 10 kHz, and initial pipet resistances were 0.4−0.8 MΩ. From a holding potential of 0 mV, currents were elicited by voltage steps to 80 mV, then to −80 mV, and back to 0 mV. Single-channel recordings were made at a sampling rate of 25 kHz, low-pass filtered at 1 kHz, and initial pipet resistances were 1.5−1.8 MΩ. For both macroscopic and single-channel recordings, the intracellular and extracellular solutions typically contained 130 mM NaCl, 0.2 mM EDTA, and 3 mM HEPES (pH 7.2). The EDTA was withheld from the solutions where indicated (−EDTA). On the basis of the algorithm in CHELATOR,[28] the expected free calcium concentrations for the different extracellular solutions were as follows: +EDTA, 2.8×10^{-7} M; −EDTA, 1×10^{-4} M. Previously performed enzyme kinetic experiments involving A3 homomeric channels and 10 nM MMP9[16] produce the following estimates of maximal MMP9 activities (V_{max}) in the presence and absence of chelator (expressed as proteolytic cleavage events): +EDTA, 7 ± 2.0 events μm^{-2} min^{-1}; −EDTA, 50 ± 15 events μm^{-2} min^{-1}. The cyclic nucleotides, cAMP and cGMP (Sigma-Aldrich, St. Louis, MO), were added to intracellular solutions as indicated. The intracellular solution applied to the face of the patch was changed using an RSC-160 rapid solution changer (Molecular Kinetics, Indianapolis, IN). Stock solutions of active human recombinant MMP9 (EMD Millipore, Billerica, MA) were diluted to 1 μg/mL with the extracellular (pipet) solution and added to the patch electrode prior to patch-clamp recording. The MMP stock solutions included 10 mM $CaCl_2$.

For native rod CNG channel recordings, retinas were dissected from *X. laevis* and placed in a frog Ringer's solution [111 mM NaCl, 2.5 mM KCl, 1 mM $CaCl_2$, 1.2 mM $MgCl_2$, 10 mM D-glucose, 0.2 mM EDTA, and 3 mM HEPES (pH 7.6)]. Rod outer segments were isolated by gentle mechanical agitation of the retinal tissue and allowed to settle in the recording chamber (i.e., a noncoated polystyrene tissue culture dish). Patch-clamp experiments were performed in the inside-out configuration as described above. In the event the rods detached from the chamber floor during patch excision (maintaining a "cell-attached" configuration), excision was facilitated by gently tapping the pipet electrode holder. Initial pipet resistances were 3−6 MΩ.

Data Analysis. Currents were leak subtracted using the current traces elicited in the absence of cyclic nucleotides before the analysis. For channel activation by cGMP, dose−response data were fit with the Hill equation: $I/I_{max} = [cNMP]^{n_H}/(K_{1/2}{}^{n_H} + [cNMP]^{n_H})$, where I is the current amplitude, I_{max} is the maximal current elicited by a saturating ligand concentration, [cNMP] is the ligand concentration, $K_{1/2}$ is the apparent ligand affinity, and n_H is the Hill slope. Fitting with the Hill equation was accomplished with Octave, an open source data analysis package (http://www.octave.org), using a custom fitting routine based on the method of steepest descent.

For nonstationary fluctuation analysis, mean isochrone current variances across 10 current traces were measured for each cGMP concentration. The cGMP-elicited variances were subtracted by the mean current variance elicited in the absence of cyclic nucleotides. Mean variances were plotted against their respective mean macroscopic current amplitudes and were fit with the parabolic equation $\sigma^2 = Ii - (I^2/N)$, where σ^2 is the mean current variance, I is the mean macroscopic current amplitude, i is the single-channel current amplitude, and N is the number of conductive channels in the membrane patch.

To quantify the MMP-induced gating effects, the Gibbs free energy of the overall reaction of CNG channel opening (ΔG) was calculated using the equation $\Delta G = -RT \ln(1/K_{1/2}{}^{n_H})$,[29] where R is the gas constant (1.987 cal K^{-1} mol^{-1}) and T is the temperature in kelvin. The differences of the Gibbs free energy change ($\Delta\Delta G$) caused by MMP activity were calculated via the equation $\Delta\Delta G = \Delta G_{MMP} - \Delta G_{control}$.

Protein Biochemistry. Proteolysis experiments with CNGA3 and CNGA1 were performed as previously described.[16] Briefly, *Xenopus* oocytes expressing either FLAG-tagged CNGA3 or FLAG-tagged CNGA1 were exposed either to a mixture of stock MMP9 and MMP2 solutions (100 μg/mL) or to an equal volume of MMP vehicle for approximately 1 h at room temperature prior to the collection of samples. To potentially facilitate proteolysis, 1 μM CPT-cGMP was added to the reaction solution, exposing the channels to a subsaturating concentration of cGMP during MMP exposure.[16] Oocyte lysates were prepared as previously described.[27] Briefly, oocytes were placed in lysis buffer containing 20 mM HEPES (pH 7.5), 150 mM NaCl, 5 mM EDTA, 0.5% Triton X-100 (Thermo Scientific, Rockford, IL), and protease inhibitors (cOmplete, Mini, EDTA-free Protease Inhibitor Cocktail Tablets, Roche Applied Science, Penzberg, Germany). Oocytes were subjected to homogenization, and the soluble cell lysate was then separated from the yolk and other insoluble material by centrifugation at 20000 *g* for 10 min at 4 °C. The lysate representing approximately one oocyte per lane was loaded and separated by sodium dodecyl sulfate−polyacrylamide gel electrophoresis (PAGE) under reducing conditions on NuPAGE 4 to 12% Tris-acetate gels (Life Technologies, Carlsbad, CA). Proteins were then transferred to a nitrocellulose membrane using the NuPAGE transfer system (Life Technologies). Immunoblots were processed as described previously,[26] FLAG-tagged subunits were detected using an anti-FLAG M2 monoclonal antibody (Sigma-Aldrich) at a concentration of 1:50000 in TTBS buffer with 1% nonfat dry milk, followed by chemiluminescent detection (SuperSignal

dx.doi.org/10.1021/bi400824x | *Biochemistry* 2013, 52, 8352−8362

West Dura Substrate, Thermo Scientific). The approximate molecular weights of the FLAG-tagged subunits were estimated using protein standards (SeeBlue Plus2, Life Technologies).

Statistical Analysis. Analyses of variance (ANOVAs) and single pairwise and multiple pairwise comparisons were performed with NCSS statistical software (NCSS, Kaysville, UT). Data were tested for normality and equal variance prior to hypothesis testing; data that violated the assumption of equal variance were analyzed with the Mann−Whitney test as indicated. Single pairwise comparisons of normally distributed and equal-variant (NDEV) data were analyzed with the Student's t test; multiple pairwise comparisons of NDEV data were analyzed with the Holm−Bonferroni corrected t test[30] subsequent to the statistically significant ANOVA result. A p value of <0.05 was considered to be statistically significant for all hypothesis tests. All values are reported as means ± the standard error of the mean (SEM) of n experiments (patches) unless otherwise indicated.

RESULTS

MMP9 Enhances Ligand Sensitivity and Decreases the Maximal Current of Heteromeric CNGA3 and CNGB3 Channels. We examined the effects of MMP9 on CNG channel gating and rundown using inside-out patches excised from *Xenopus* oocytes expressing both CNGA3 and CNGB3 subunits. MMP9 (10 nM) was added to the patch-electrode solution, thus providing access to the extracellular surface of the membrane patch. We assessed CNG channel gating properties by measuring cGMP dose−response relationships, determining the apparent affinity for cGMP using fits with the Hill equation. Because MMP catalytic activity is dependent on association with divalent cations, including Zn^{2+} and Ca^{2+},[31] we examined the MMP-dependent changes in CNG channel activity at both high and low divalent cation concentrations, produced by omitting the chelator (−EDTA) or including EDTA (+EDTA) in the extracellular solution; the expected free calcium concentrations were 1×10^{-4} M without EDTA and 2.8×10^{-7} M with EDTA (see Experimental Procedures). As shown previously,[16] extracellular application of MMP9, in the presence of a low divalent cation concentration, increased the apparent affinity for cGMP (decreased $K_{1/2}$) relative to that of control patches (Figure 1A,B). Within 20 min of MMP exposure, both the $K_{1/2}$ cGMP (mean ± SEM; for MMP, $K_{1/2}$ = 7.4 ± 0.8 μM; for the control, $K_{1/2}$ = 15.2 ± 1.1 μM; $p < 0.001$, Student's t test, n = 5 or 7) and the Hill slope (n_H) (for MMP, n_H = 1.6 ± 0.2; for the control, n_H = 2.1 ± 0.1; $p < 0.05$, Student's t test, n = 5 or 7) were significantly reduced for MMP-treated patches. These changes in gating enhanced the current elicited by a subsaturating concentration of cGMP (2 μM) (Figure 1C). We previously demonstrated that high divalent cation concentrations accelerated the MMP-dependent gating changes in CNGA3 homomeric (A3) channels.[16] Similarly, we observed that high divalent cation concentrations accelerated MMP9-dependent effects on gating for CNGA3 and CNGB3 (A3+B3) heteromeric channels (Figure 1A,B). Within 20 min of patch excision, MMP9 in a high concentration of divalent cations effected a more profound reduction in $K_{1/2}$ cGMP ($K_{1/2}$ = 1.5 ± 0.2 μM; $p < 0.001$, Student's t test, n = 4 or 5) and the Hill slope (n_H = 0.78 ± 0.07; $p < 0.01$, Student's t test, n = 4 or 5) relative to those of MMP9 in a low concentration of divalent cations. In addition to the changes in channel gating, prolonged exposure to MMP9 promoted a decrease in the maximal cGMP-elicited current (I_{max} rundown) that was also accelerated and enhanced by high divalent cation concentrations (Figure 1C,D). Within 40 min of patch excision, the MMP-treated patches (−EDTA) exhibited considerable I_{max} rundown relative to control patches (for MMP, $I_{max}/I_{max,T_0}$ = 0.31 ± 0.03; I_{max}/

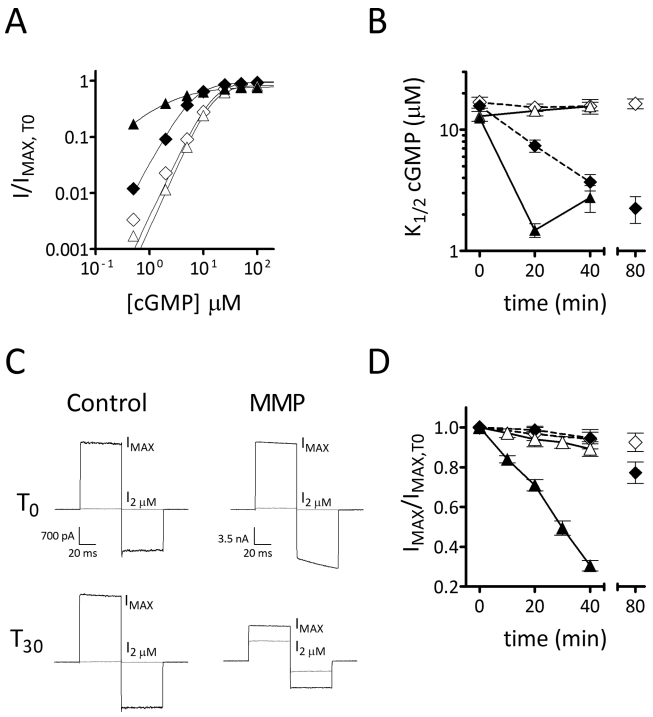

Figure 1. MMP9 enhances ligand sensitivity and decreases the maximal current of heteromeric A3+B3 channels. (A) Representative dose−response relationships for activation of A3+B3 channels by cGMP 20 min after excision for control (empty symbols) and ∼10 nM MMP9-treated (filled symbols) patches. For these recordings, EDTA (0.2 mM) was present (+EDTA, diamonds) or absent (−EDTA, triangles) in the extracellular solution, thus influencing the availability of free divalents. Currents were measured with an applied voltage of 80 mV and normalized to the initial maximal cGMP current (I_{max}); currents in the absence of cGMP were subtracted. Solid curves represent fits using the Hill equation, as described in Experimental Procedures, with the following best-fit parameters: for the control with EDTA, $K_{1/2,T_{20}}$ = 15.3 μM and $n_{H,T_{20}}$ = 2.0; for MMP with EDTA, $K_{1/2,T_{20}}$ = 6.5 μM and $n_{H,T_{20}}$ = 1.8; for the control without EDTA, $K_{1/2,T_{20}}$ = 15.2 μM and $n_{H,T_{20}}$ = 2.2; for MMP without EDTA, $K_{1/2,T_{20}}$ = 2.0 μM and $n_{H,T_{20}}$ = 0.9. (B) Time course for the change in the cGMP apparent affinity for control (empty symbols) and MMP-treated (filled symbols) patches following excision. Patch recordings were taken in the presence (diamonds, hashed lines) or absence (triangles, solid lines) of extracellular EDTA. Data were based on best-fit Hill curves and expressed as mean $K_{1/2}$ ± SEM. (C) Representative current traces for control and MMP9-treated channels (in the absence of EDTA), after activation by a saturating (I_{max}, black line) or subsaturating ($I_{2\mu M}$, gray line) concentration of cGMP, immediately (top, T_0) and 30 min (bottom, T_{30}) following patch excision. Current traces were elicited using voltage steps from a holding potential of 0 mV, to 80 mV, to −80 mV, and then to 0 mV and were normalized to the maximal T_0 current. MMP9 increased the current in subsaturating cGMP despite a decrease in the maximal current. (D) Change in the maximal cGMP-elicited current as a function of time following patch excision for control (empty symbols) and MMP9-treated (filled symbols) patches in the presence (diamonds) or absence (triangles) of extracellular EDTA. Currents were normalized to I_{max} at the time of patch excision (I_{max,T_0}).

dx.doi.org/10.1021/bi400824x | *Biochemistry* 2013, 52, 8352−8362

I_{max,T_0} = 0.89 ± 0.04). Taken together, these data suggest that MMP-dependent proteolysis is antecedent to both the enhanced ligand sensitivity and I_{max} rundown of A3+B3 heteromeric channels.

MMP-Dependent I_{max} Rundown Is Due to the Loss of Conductive Channels. The macroscopic current amplitude (I) is determined by the single-channel current (i), the number of conductive channels (N), and the open probability (P_O), where $I = iNP_O$. Accordingly, MMP exposure may promote I_{max} rundown by decreasing the number of conductive channels, the single-channel conductance, or the maximal open probability. To distinguish between these possibilities, we analyzed the current−variance relationship of MMP-treated A3+B3 heteromeric channels (see Experimental Procedures). If the MMP-mediated I_{max} rundown is due to a decrease in the maximal open probability, we would expect to see an increase in the current variance at saturating cGMP (as $P_{O,max}$ approaches 0.5). However, the current variance in saturating cGMP decreases with I_{max} rundown (Figure 2A,B). This decrease in the current variance during I_{max} rundown was also observed for A3 homomeric channels (data not shown). The linear relationship between the variance and I_{max} rundown is consistent with a decrease in conductive channels.

To further examine the nature of the I_{max} rundown, we examined the single-channel activity of MMP9-treated A3 channels in the presence of a saturating concentration of cGMP (1 mM). With extended exposure to MMP9, we observed discrete reductions in current equivalent to the estimated single-channel current amplitude (mean ± standard deviation; Δi = −3.6 ± 0.5 pA) (Figure 2C−E). However, MMP exposure did not reduce the estimated single-channel current amplitude (before reduction, i = 3.5 ± 0.5 pA; after reduction, i = 3.5 ± 0.6 pA; $p > 0.10$, Student's t test, n = 3) or the maximal open probability (before reduction, $P_{O,max}$ = 0.97 ± 0.02; after reduction, $P_{O,max}$ = 0.99 ± 0.003; $p > 0.1$, Student's t test, n = 3) for the remaining conductive channels. Collectively, these results indicate that the MMP-dependent I_{max} rundown is due to a loss of conductive channels (decreased N) rather than a decrease in the single-channel current amplitude or the maximal open probability.

CNGA3 N-Glycosylation Protects against MMP-Dependent Processing. Intriguingly, we observed a reversal of $K_{1/2}$ cGMP to control levels after extended MMP exposure (40−60 min) under conditions of enhanced MMP activity (i.e., high divalent cation concentration). This recovery in $K_{1/2}$ cGMP was observed for both A3+B3 heteromeric (Figure 3A) and A3 homomeric channels (Figure 3B). Because of the temporal variation across experiments, we summarized the gating effects by binning $K_{1/2}$ cGMP for Initial (at time of excision), Peak (at maximal gating effect), and approximate End point (35 to 20% of the Initial I_{max}). The $K_{1/2,GMP}$ values at these binned groups were as follows (mean ± SEM): for A3+B3 heteromeric channels, Initial = 11.8 ± 1.0 μM, Peak = 1.2 ± 0.1 μM, and End point = 10.0 ± 2.8 μM; for A3 homomeric channels, Initial = 5.6 ± 1.0 μM, Peak = 0.15 ± 0.03 μM, and End point = 8.6 ± 0.6 μM. The changes in $K_{1/2}$ cGMP were accompanied by corresponding changes in cAMP efficacy for both channel compositions (data not shown). These results imply a reversion of channel gating properties to control levels (i.e., gating reversion) with extended MMP exposure.

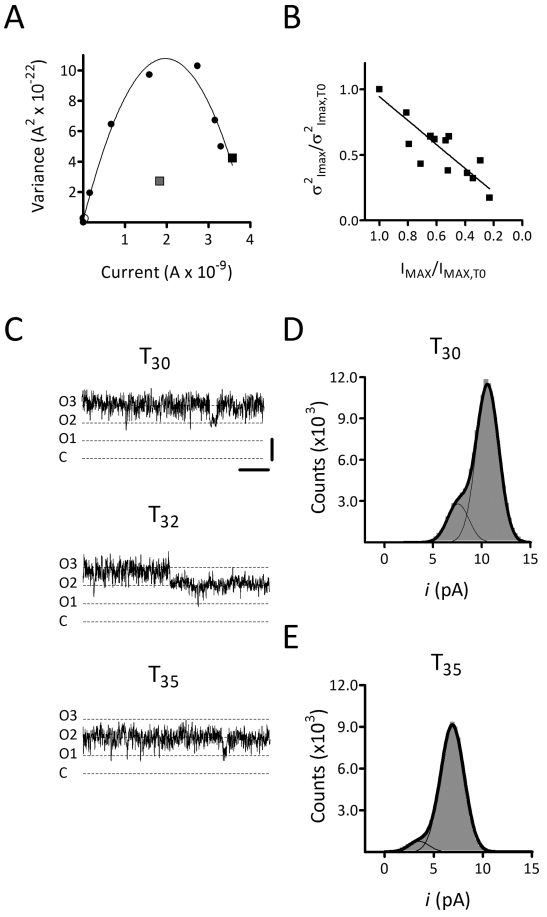

Figure 2. MMP-dependent I_{max} rundown is due to loss of conductive channels. (A) Representative current−variance relationships for MMP9-treated A3+B3 channels immediately following excision (T_0, black symbols) and ∼30 min following excision (T_{30}, gray symbol). The black line was produced by fitting the T_0 current−variance data with a second-order polynomial (see Experimental Procedures). Squares denote the current and variance at a saturating concentration of cGMP ($\sigma^2_{I_{max}}$) for T_0 and T_{30}. Note the divergence along the vertical axis between the T_{30} $\sigma^2_{I_{max}}$ (gray square) and the predicted curve. (B) Regression analysis between the change in I_{max} ($I_{max}/I_{max,T_0}$) and the change in the I_{max} current variance ($\sigma^2_{I_{max}}/\sigma^2_{I_{max,T0}}$) for MMP-treated A3+B3 channels. Data were pooled from three independent time courses for MMP-treated A3+B3 channels (−EDTA). Current variance in saturating cGMP decreases linearly with I_{max} rundown (slope of 0.91 ± 0.1; F test, $p < 0.001$, n = 15); note the inverted X-axis. (C) Representative traces are shown for an inside-out patch containing three CNGA3-only (A3) channels in a saturating concentration of cGMP (1 mM) at ∼30 min (T_{30}; top), ∼32 min (T_{32}; middle), and ∼35 min (T_{35}; bottom) following patch excision. Currents were recorded at a membrane potential of 80 mV. C represents the closed channel mean current level; O represents the current level(s) for the open channel(s). Horizontal and vertical scale bars denote 50 ms and 5 pA, respectively. The T_{32} current trace exhibits a persistent loss of current amplitude approximately equal to the unitary current. Current amplitude histograms for T_{30} (D) and T_{35} (E) time points were amassed from 4 to 6 s of recording and fit with the sum of two Gaussian functions. The best-fit Gaussian curves produced the following maximal open probabilities ($P_{O,max}$), maximal collective current (I_{max}), and single-channel current amplitude (i) estimates: at T_{30}, $P_{O,max}$ = 0.94, I_{max} = 10.6 pA, and i = 3.5 pA; at T_{35}, $P_{O,max}$ = 0.98, I_{max} = 6.9 pA, and i = 3.5 pA. These results are representative of three independent patches.

dx.doi.org/10.1021/bi400824x | Biochemistry 2013, 52, 8352−8362

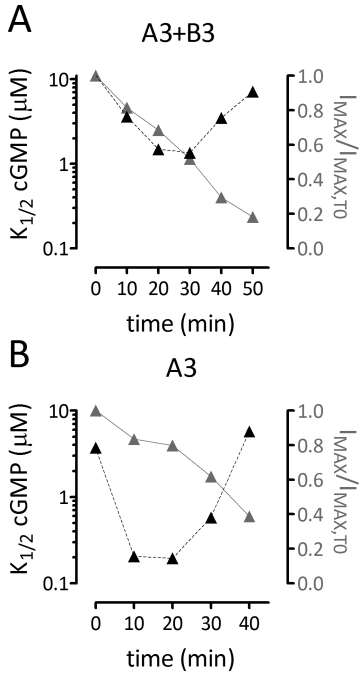

Figure 3. Enhanced MMP-dependent processing of channels produces a gating reversion concomitant with I_{max} rundown. Representative time courses are shown for the MMP-dependent change in the apparent cGMP affinity of MMP-treated heteromeric A3+B3 (A) and homomeric A3 (B) channels. Data were collected in the absence of extracellular EDTA. For each plot, $K_{1/2}$ cGMP (black triangles, left axis) and I_{max} relative to I_{max,T_0} (gray triangles, right axis) are shown.

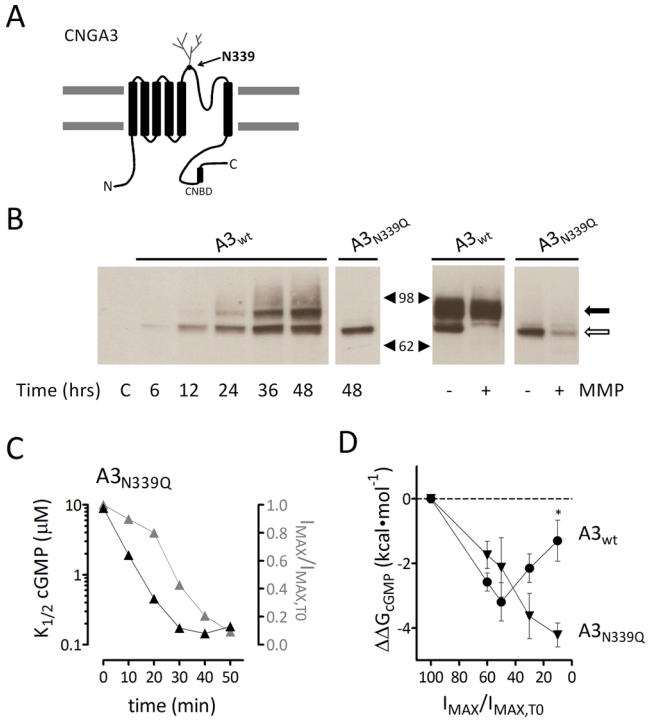

Figure 4. Elimination of CNGA3 N-glycosylation diminishes the level of gating reversion. (A) CNGA3 subunits contain one core N-glycosylation site (N339), which is located in the pore turret. CNBD denotes the cyclic nucleotide binding domain. (B) Protein glycosylation can be protective against proteolytic modification by MMP. Immunoblot analysis of protein lysates from oocytes expressing FLAG-CNGA3$_{wt}$ or FLAG-CNGA3$_{N339Q}$ subunits. Time course for expression of glycosylated (filled arrow) and nonglycosylated/core-glycosylated (open arrow) CNGA3 subunits (left), and of *in vitro* A3$_{wt}$ and A3$_{N339Q}$ subunit proteolysis by MMPs (right). *C* denotes control uninjected oocytes. Protein immunoreactivity was assessed using the anti-FLAG antibody. For *in vitro* proteolysis experiments, intact oocytes were treated with MMP2 and -9 (100 μg/mL total) for 1 h, approximately 4 days following mRNA injection. (C) Representative time course for the MMP-dependent change in $K_{1/2}$ cGMP (black triangles, left axis) and I_{max} (gray triangles, right axis) for A3$_{N339Q}$ channels in the absence of EDTA in the electrode solution (−EDTA). (D) Summary of effects of MMP on the change in free energy difference for channel gating [$\Delta\Delta G_{cGMP}$ (see Experimental Procedures)] relative to I_{max} rundown for A3$_{wt}$ (●) and A3$_{N339Q}$ (▼) channels. All recordings were taken in the absence of EDTA. $\Delta\Delta G_{cGMP}$ values were binned at various levels of the fractional change in I_{max}. The rebound in ligand sensitivity was significantly reduced for A3$_{N339Q}$ compared to that for A3$_{wt}$ (*p < 0.05, Student's t test, n = 7).

These results were surprising as we expected proteolytic modification of core channel subunits to irreversibly affect channel function. One possible explanation for these observations is that the apparent gating reversion arises from a subset of the CNG channels being resistant to the MMP-mediated gating changes and eventual loss of conductivity. Accordingly, the loss of MMP-modified channels (underlying I_{max} rundown) would increase the relative contribution of the resistant, nonmodified channels to the macroscopic current. Human CNGA3 subunits possess a single N-glycosylation site within the pore turret [N339 (Figure 4A)]. Because glycosylation can impart protection against substrate proteolysis,[32−35] we hypothesized that CNGA turret glycosylation confers resistance to MMP-dependent processing. To test this hypothesis, we utilized a CNGA3 mutant lacking the N339 turret glycosylation site (A3$_{N339Q}$). First, we exposed intact oocytes expressing wild-type CNGA3 (A3$_{wt}$) or A3$_{N339Q}$ channels to MMPs for 1 h. Via immunoblot analysis, we observed a loss of the full-length channel subunits for both the nonglycosylated/core-glycosylated form of the A3$_{wt}$ subunits and the A3$_{N339Q}$ subunits (Figure 4B). Conversely, glycosylated A3$_{wt}$ subunits were relatively resistant to MMP-dependent proteolysis (Figure 4B).

Next, we investigated the effects of MMP exposure on gating and I_{max} rundown of A3$_{N339Q}$ channels. We predicted that if pore turret glycosylation protects against MMP-dependent modifications, then removal of the glycosylation site will reduce or eliminate the protected subpopulation, thereby attenuating the observed gating reversion. Similar to what was observed for A3$_{wt}$ channels, MMP exposure increased the ligand sensitivity and promoted I_{max} rundown of A3$_{N339Q}$ channels. However, even with extensive I_{max} rundown, A3$_{N339Q}$ channels did not exhibit an obvious reversal in ligand sensitivity (Figure 4C). To quantitatively compare the extent of gating reversion between A3$_{wt}$ and A3$_{N339Q}$ channels, we calculated the MMP-dependent changes in the free energy difference of the channel opening transition ($\Delta\Delta G$, where $\Delta\Delta G = \Delta G_{MMP} - \Delta G_{control}$) for each channel composition (see Experimental Procedures). Subsequent to the maximal MMP-dependent change in gating ($\Delta\Delta G \approx -3$ kcal/mol), the $\Delta\Delta G$ for A3$_{wt}$ channels increased to approximately −1 kcal/mol at low $I_{max}/I_{max,T_0}$ values, signifying a profound gating reversion with extensive I_{max} rundown (Figure 4D). In contrast, the $\Delta\Delta G$ for MMP-treated A3$_{N339Q}$ channels progressively decreased to approximately −4 kcal/mol at low $I_{max}/I_{max,T_0}$ values, indicating that the gating reversion was

dx.doi.org/10.1021/bi400824x | *Biochemistry* 2013, 52, 8352−8362

virtually absent for $A3_{N339Q}$ channels (Figure 4D). We observed a similar effect with oocytes expressing $A3_{wt}$ channels that were treated with tunicamycin, an inhibitor of N-glycosylation (data not shown). Furthermore, the gating properties and time-dependent changes in I_{max} for untreated $A3_{N339Q}$ channels were not significantly different from those of untreated $A3_{wt}$ channels (data not shown). Collectively, these results suggest that the observed reversion in ligand sensitivity of MMP-modified $A3_{wt}$ channels is likely due to the emerging contribution of MMP-resistant channels, and that N-glycosylation within the pore turret confers this resistance.

Position of the CNGA Glycosylation Site within the Pore Turret Determines Whether CNG Channels Are Protected from MMP-Dependent Modification. Native rod photoreceptor CNG channels are heterotetramers containing CNGA1 and CNGB1 subunits. To characterize the MMP-dependent change in ligand sensitivity and I_{max} rundown of rod CNG channels, we examined the effects of MMP9 on expressed bovine CNGA1 homomeric channels (A1) or CNGA1 co-expressed with human CNGB1 (A1+B1). Similar to CNGA3 subunits, CNGA1 subunits possess a single N-glycosylation site within the pore turret.[23] Unlike that of CNGA3 subunits, immunoblot analysis of FLAG-tagged CNGA1 subunits suggests that the glycosylated and non-glycosylated forms of the subunit are equally susceptible to *in vitro* MMP9 proteolysis, in the context of homomeric A1 or heteromeric A1+B1 channels (Figure 5A). Next, we examined the relationship between the MMP-mediated I_{max} rundown and the apparent gating reversion (i.e., emergence of a protected subpopulation) for A1 channels. In contrast to A3 channels, gating reversion was nearly absent for A1 channels (Figure 5B). For A3 channels, gating reversion is apparent as I_{max} approaches ~50% of the initial amplitude, and nearly complete reversion is apparent at ~10% of the initial I_{max}. However, A1 channels exhibit only a partial reversion at ~10% of the initial I_{max} (Figure 5C).

Next we tested whether CNGA1 glycosylation is ineffective at protecting A1+B1 heteromeric channels from MMP-dependent gating changes. We monitored the MMP-dependent changes in gating for patches that contained heterologously expressed A1+B1 channels and patches containing native A1+B1 channels excised from *Xenopus* rod outer segments. Similar to A1 homomeric channels, the heterologously expressed A1+B1 heteromeric channels lacked a distinct gating reversion with I_{max} rundown (Figure 5D). Unexpectedly, *Xenopus* rod A1+B1 channels demonstrated a profound gating reversion (Figure 5D), which was comparable to the reversion observed with CNGA3-containing channels (see Figure 3).

Interestingly, protein sequence alignments for the turret region of homologous channel subunits indicate that CNGA glycosylation occurs at two distinct positions within the pore turret: the bovine CNGA1 glycosylation site (position 1) is shifted toward the amino terminus in relation to other paralogs and orthologs, including that of *Xenopus* CNGA1 (position 2) (Figure 6A). This led us to hypothesize that the location of the glycosylation site within the pore turret determines whether CNG channels are protected from MMP-dependent processing. To test this hypothesis, we utilized a bovine CNGA1 mutant engineered to relocate the glycosylation site to position 2, which is the glycosylation site found in human CNGA3 and *Xenopus* CNGA1: N337T, D344N, and N346S ($CNGA1_{NDN\text{-}TNS}$) (Figure 6A). In contrast to channels containing wild-type CNGA1 subunits, channels containing

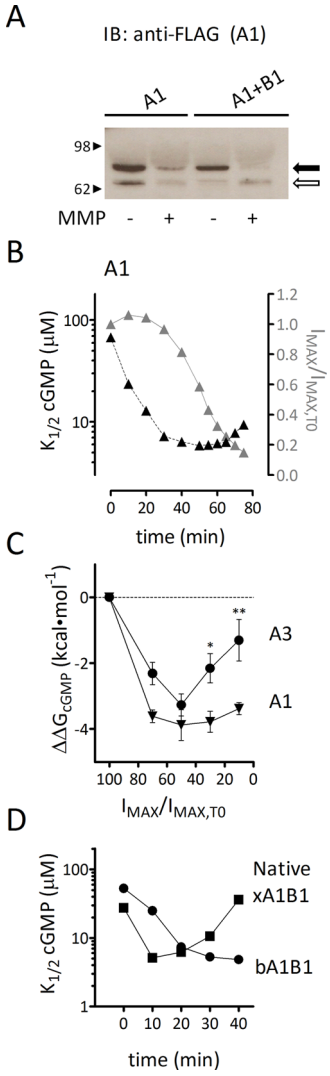

Figure 5. CNGA1 N-glycosylation is only nominally protective against MMP-dependent subunit proteolysis and gating effects. (A) Immunoblot analysis of FLAG-tagged CNGA1 (A1) subunits suggests that the glycosylated (filled arrow) and nonglycosylated/core-glycosylated (open arrow) forms of the subunit are both susceptible to *in vitro* MMP proteolysis, in the context of either homomeric A1 or heteromeric A1+B1 channels. Protein immunoreactivity was assessed using the anti-FLAG antibody, and intact oocytes were treated as described in the legend of Figure 4B. (B) Representative time course for the MMP-dependent change in the apparent cGMP affinity (black triangles, left axis) and I_{max} (gray triangles, right axis) of A1 homomeric channels. (C) Summary of the effects of MMP on $\Delta\Delta G_{cGMP}$ in relation to I_{max} for A1 and A3 homomeric channels. The rebound in ligand sensitivity was significantly reduced for A1 channels compared to that for A3 channels (*p < 0.05, **p < 0.01, Holm's t test, n = 5–13). (D) Representative time courses for the change in $K_{1/2}$ cGMP for patches with heterologously expressed A1+B1 channels (comprised of bovine CNGA1 and human CNGB1 subunits) and patches containing native A1+B1 channels excised from *Xenopus* rod outer segments. Native *Xenopus* channels exhibited a pronounced gating reversion with extensive I_{max} rundown ($I_{max}/I_{max,T_0} \approx 0.25$ at the conclusion of the time course for both representative patches; MMP-dependent changes in I_{max} are not shown for the sake of clarity).

$CNGA1_{NDN\text{-}TNS}$ subunits exhibited a robust gating reversion following extensive I_{max} rundown with MMP exposure (Figure 6B); $A1_{NDN\text{-}TNS}$ channels also exhibited a reduced maximal

dx.doi.org/10.1021/bi400824x | *Biochemistry* 2013, 52, 8352–8362

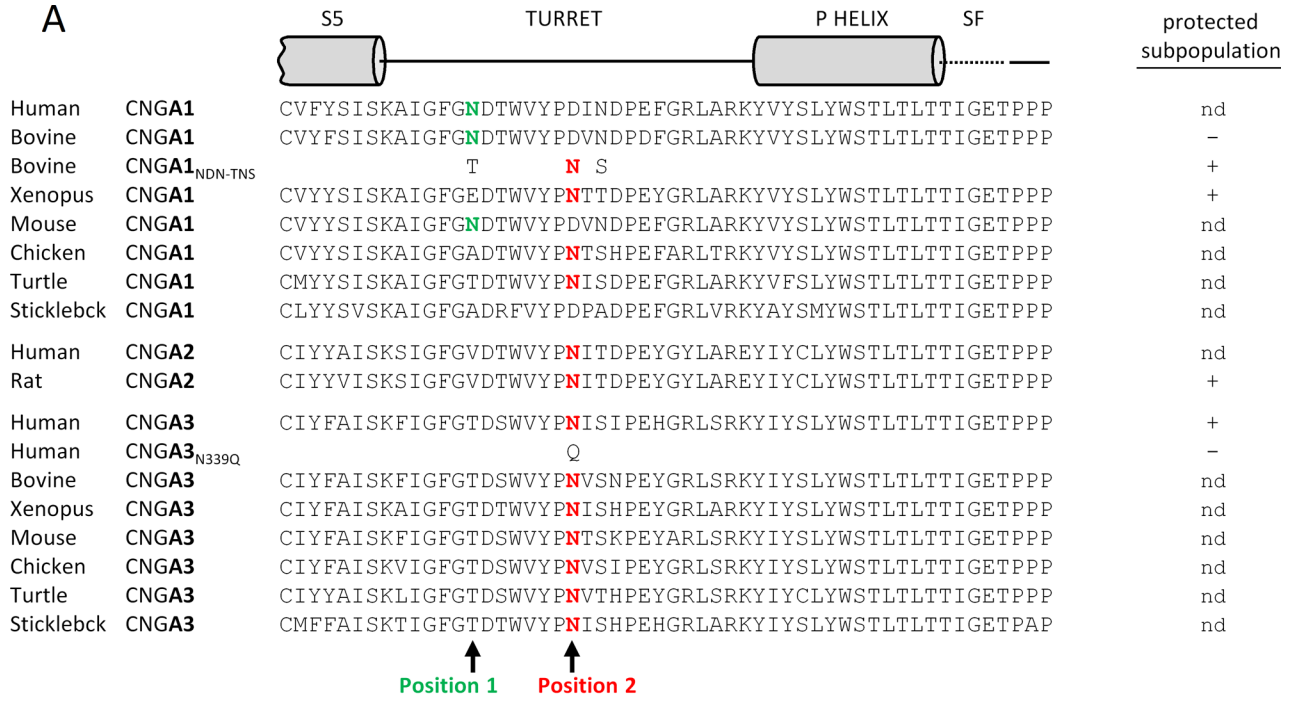

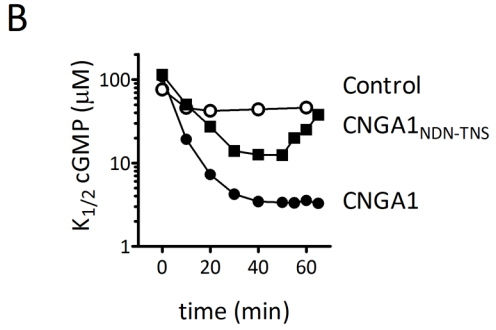

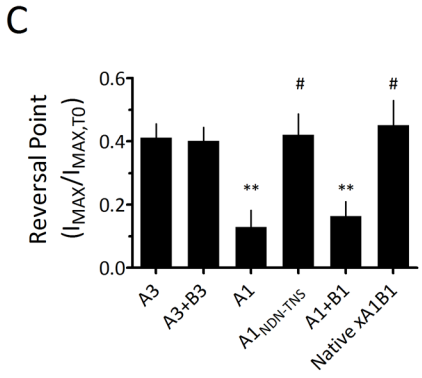

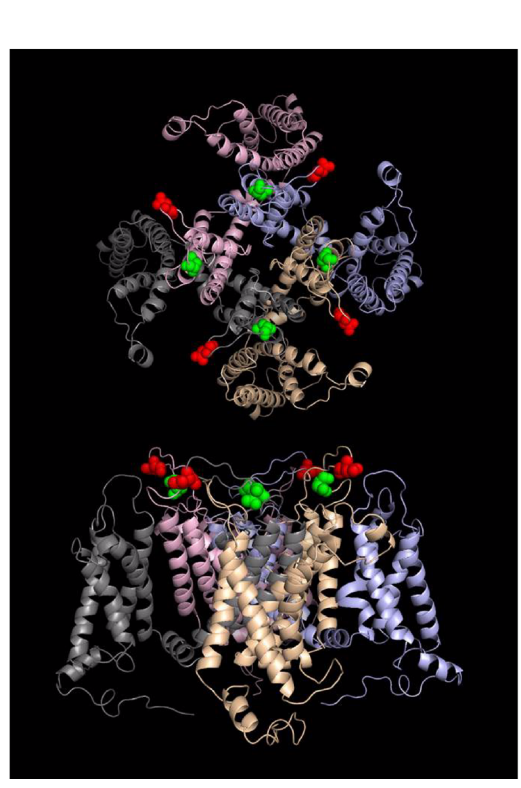

Figure 6. Location of the glycosylation site within the pore turret determines whether CNG channels are protected from MMP-dependent processing. (A) Sequence alignment for various CNGA subtypes. Locations of conserved N-glycosylation sites are shown in bold. Homomeric channels comprised of rat CNGA2 subunits exhibit a gating reversion comparable to that of channels comprised of human CNGA3 subunits (data not shown). A plus sign indicates a substantial fraction of protected channels; a minus sign indicates a limited presence of protected channels, and nd indicates that the presence of protected channels has not been determined. The accession or entry numbers for the sequences shown are as follows: for CNGA1, NP000078.2 (*Homo sapiens*), NP776703.1 (*Bos taurus*), AAH93579.1 (*X. laevis*), NP031749.2 (*Mus musculus*), NP990551.1 (*Gallus gallus*), K7FWR1 (*Pelodiscus sinensis*), and G3N531 (*Gasterosteus aculeatus*); for CNGA2, NP005131.1 (*H. sapiens*) and NP037060.1 (*Rattus norvegicus*); for CNGA3, NP001289.1 (*H. sapiens*), NP776704.1 (*B. taurus*), XP004911865.1 (*Xenopus tropicalis*), NP034048.1 (*M. musculus*), NP990552.1 (*G. gallus*), K7GE18 (*P. sinensis*), and G3PKL4 (*Ga. aculeatus*). (B) Representative time courses for the change in $K_{1/2}$ cGMP for channels containing bovine $CNGA1_{wt}$ [control (○) and MMP-treated (●)] and a bovine CNGA1 mutant constructed to move the glycosylation site

dx.doi.org/10.1021/bi400824x | *Biochemistry* 2013, 52, 8352−8362

Figure 6. continued

(position 1) to a site homologous to the human CNGA3 glycosylation site: N337T, D344N, and N346S [$CNGA1_{NDN\text{-}TNS}$ (■)] (position 2). Channels comprised of $CNGA1_{NDN\text{-}TNS}$ exhibited a pronounced gating reversion with extensive I_{max} rundown ($I_{max}/I_{max,T_0} \approx 0.2$ at the conclusion of the time course for both MMP-treated patches; MMP-dependent changes in I_{max} are not shown for the sake of clarity). (C) Extent of I_{max} rundown, relative to T_0 I_{max}, necessary for the onset of the gating reversion (i.e., I_{max} reversal point). Homomeric and heteromeric channels comprised of bovine CNGA1 required a greater extent of I_{max} rundown to exhibit a gating reversion (i.e., a reduced I_{max} reversal point) compared to channels comprised of human CNGA3 ($p < 0.0001$, single-factor ANOVA; $^{**}p < 0.01$, Holm's t test, $n = 5-10$) and *Xenopus* CNGA1 ($^{\#}p < 0.05$, Holm's t test, $n = 5$ or 6). A reduced I_{max} reversal point for bovine $CNGA1_{wt}$-containing channels reflects a less abundant protected population relative to that of CNGA3-containing channels. Furthermore, repositioning the bovine CNGA1 glycosylation site to a position homologous with that of the human CNGA3 site increased the relative abundance of protected channels, as evidenced by the elevated I_{max} reversal point for $A1_{NDN\text{-}TNS}$ channels relative to $A1_{wt}$ channels ($^{\#}p < 0.05$, Holm's t test, $n = 5$ or 6). (D) Model of the CNG channel structure (S1−S6) showing the relative positions of bovine CNGA1 (position 1) vs CNGA3 (position 2) glycosylation sites. The human CNGA1 model is viewed from the extracellular side of the membrane (top), and through the plane of the membrane, with the extracellular region above and the cytoplasmic region below (bottom). The spheres represent the positions of asparagine residues within the glycosylation sequons for position 1 (green) and position 2 (red). The S5−S6 segments of CNGA1 were rendered using the crystal structure of KvAP and SWISS-MODEL[62−64] [Protein Data Bank (PDB) entry 1ORQ]. The rendered S5−S6 fragment was subsequently docked to the crystal structure of the S1−S4 fragment of the Shaker potassium channel Kv1.2 (PDB entry 3LUT) in Pymol. The Kv1.2 S1−S2 linker was altered to match the length of the CNGA1 S1−S2 linker.

change in apparent cGMP affinity compared to that of $A1_{wt}$ channels ($K_{1/2}$ cGMP at Peak of gating effect: for $A1_{NDN\text{-}TNS}$, $K_{1/2} = 16.1 \pm 4.3$ μM; for $A1_{wt}$, $K_{1/2} = 3.5 \pm 1.8$ μM; $p < 0.05$, Mann−Whitney test, $n = 5$). The reduced maximal change in $K_{1/2}$ cGMP for $A1_{NDN\text{-}TNS}$ channels is likely due to an increased contribution of unmodified channels to the macroscopic dose−response relationship. For control (untreated) $A1_{wt}$ channels, the previously characterized increase in ligand sensitivity (run up) associated with tyrosine dephosphorylation[6] was observed (Figure 6B). The NDN-TNS mutations did not alter the gating properties, run up in ligand sensitivity, or time-dependent changes in I_{max} for untreated channels (data not shown). In our experiments, gating reversion was reduced or eliminated in instances where the glycosylation site was absent ($CNGA3_{N339Q}$) or located at position 1 (bovine $CNGA1_{wt}$) (Figure 6C). Collectively, these results indicate that the location of the glycosylation site is an important determinant influencing whether CNG channels are protected from MMP-dependent processing.

■ DISCUSSION

Two contrasting events are associated with MMP-dependent modifications to CNG channels: increased ligand sensitivity and a loss of conducting channels. MMPs are known to have many extracellular and pericellular substrates, making it plausible that MMPs alter CNG channel activity indirectly through other signaling systems (e.g., integrins and ICAM).[36,37] Although we cannot rule out indirect contributions to the gating changes, previous experiments indicated that the MMP-dependent gating effects likely arise from direct proteolysis of core channel subunits.[16] In accordance with previous observations,[16] these gating effects increased the current in 2 μM cGMP, which is the approximate physiological cGMP concentration in photoreceptors in the dark.[38] Concomitant with the increased ligand sensitivity is a reduction in the Hill slope of cGMP dose−response curves (see Figure 1). Analyses of cGMP dose−response curves and current fluctuations suggest that MMPs generate CNG channel subpopulations by sequentially modifying individual CNGA subunits, where the apparent affinity for cGMP is governed by the total number of modified subunits (from 0 to 4) (S. E. Meighan, P. C. Meighan, and M. D. Varnum, unpublished observations). The heterogeneous ligand sensitivities produced by differentially modified CNG channels would cause a reduction in the Hill slope for cGMP dose−response curves. Consistent with this, it has been reported previously that heterogeneous gating properties likely account for differences in the Hill slope between single-channel recordings and macroscopic current recordings of CNG channels.[39] With prolonged MMP exposure, we observed a reduction in the maximal current. Single-channel recordings and macroscopic current fluctuations indicate that the current loss is apparently due to a loss of conductive CNG channels. This suggests that MMP-processed channels become nonfunctional or enter a nonconductive or persistently closed state. On the basis of the temporal relationship between the gating effects and the I_{max} rundown, we suspect that the biochemical events producing the loss of conductivity occur subsequent to the proteolytic events underlying the gating change.

For the channels examined here, multiple CNGA subunits are potentially available for processing by MMPs. One possible mechanism for the loss of conductivity is that proteolysis of a critical number of subunits facilitates entry of the channel into a nonconductive state. Another possibility is that the proteolysis underlying the gating modification may facilitate secondary cleavage events, by MMPs or other endogenous proteases, rendering the channel nonconductive. Sequential processing by multiple proteases has been described previously in other systems. For example, extracellular cleavage of receptor-like protein-tyrosine phosphatases by metalloproteinases is antecedent to intracellular cleavage by presenilin/γ-secretase.[40] Future experiments will aim to characterize the loss of CNG channel conductivity with MMP proteolysis.

The MMP-dependent I_{max} rundown revealed a subpopulation of channels that were protected from MMP-dependent processing; that protection was dependent on CNGA subunit glycosylation. There are several means by which channel glycosylation may confer resistance to MMP-dependent processing. One possibility is that glycosylation induces an allosteric effect, indirectly preventing access to an MMP cleavage site. This seems unlikely because glycosylation does not alter the gating properties of CNG channels in the absence of MMP treatment. Instead, we postulate that CNGA glycosylation sterically hinders access to the MMP cleavage site(s). In other systems, it has been demonstrated that protein glycosylation can inhibit proteolysis and attendant changes to protein function. For example, N-glycosylation interferes with trypsin-mediated digestion of an intestinal anion exchange protein (SLC26A3), consequently promoting its functional expression.[41] In addition, N-glycosylation of glutamate receptor

dx.doi.org/10.1021/bi400824x | *Biochemistry* 2013, 52, 8352−8362

GluR3 subunits interferes with specific cleavage by granzyme B and the subsequent formation of autoimmune products.[42] Depending on the channel type (rod vs cone) and configuration (homomeric vs heteromeric), the CNG channels examined here contain two to four CNGA subunits per channel. Therefore, each CNG channel likely contains multiple MMP substrates. How might CNGA glycosylation protect against proteolytic modification of CNG channel subunits? We envision two potential mechanisms for protection against MMP-dependent processing. One potential mechanism is that CNGA glycosylation confers resistance on a subunit-by-subunit basis. For the glycosylation sequons of the channels examined here, the glycosylation efficiency is expected to vary from ~50% (e.g., human CNGA3) to ~85% (e.g., bovine CNGA1).[43] On the basis of these efficiencies, it is likely that CNG channels exhibit a range of glycosylations (from zero to four subunits). Therefore, if glycosylation is protective of individual subunits only, protection from MMPs would exist in degrees (depending on the number of glycosylated subunits). Another potential mechanism is that CNGA glycosylation precludes access of MMPs to the extracellular channel face. In this scenario, channels that are incompletely glycosylated (i.e., containing unglycosylated CNGA subunits) may still be protected from MMP-dependent processing. Future experiments may help distinguish between these possible mechanisms.

The location of the CNGA glycosylation site within the pore turret critically determines whether channels are protected from MMP-dependent processing. There is a nearly uniform location for CNGA2 and CNGA3 turret glycosylation at position 2 (Figure 6A). In contrast, CNGA1 turret glycosylation sites exhibit greater heterogeneity among orthologs: most mammals present position 1 glycosylation sites in CNGA1; birds, amphibians, and reptiles present position 2 sites; and many fish CNGA1 orthologs entirely lack a turret glycosylation site. For bovine CNGA1, as in other mammalian CNGA1 orthologs, the position 1 glycosylation site is shifted by seven amino acids toward the N-terminus relative to the position 2 site (e.g., human CNGA3 and *Xenopus* CNGA1). On the basis of a composite model of human CNGA1 using the crystal structures of KvAP and the Shaker potassium channel Kv1.2 (Protein Data Bank entrie 1ORQ and 3LUT, respectively), this shift may dramatically alter the orientation and position of the glycosylation site relative to the other parts of the channel (Figure 6D). Interestingly, the position 1 glycosylation site is centrally oriented on the pore turret loop, whereas the position 2 site is tethered more closely to S5. This positional difference would seemingly permit CNGA3 glycosylations to cover a wider area of the channel surface compared to bovine CNGA1 glycosylation, potentially influencing access of MMPs to the channel. Alternatively, the difference in susceptibility to MMP-mediated proteolysis may be due to differences in proximity between CNGA glycosylation sites and a specific MMP cleavage site(s). Possible MMP cleavage sites, for which access might be differentially occluded by position 2 versus position 1 glycosylation, include the extracellular S1−S2 loop and the pore turret itself. Further studies are necessary to fully elucidate the mechanism by which glycosylation protects against MMP-dependent proteolysis.

It has been demonstrated previously that the absence of CNGA pore turret glycosylation does not impact the functional properties of CNG channels.[23,24] This is surprising given that pore turret glycosylation is remarkably conserved across CNG channel paralogs and orthologs (see Figure 6A), and that functionally important pore turret glycosylation sites have been characterized for several other members of the voltage-gated channel superfamily.[44] For example, interference of pore turret glycosylation disrupts targeting of HCN2 channels to the plasma membrane,[20] alters capsaicin sensitivity of TRPV1 channels,[21] and decreases the open probability of the inward rectifier potassium channel, ROMK1.[22] How might CNGA pore turret glycosylation impact CNG channel function in photoreceptors? We speculate that the CNGA glycosylation regulates susceptibility to processing by retinal MMPs, which have been localized within the interphotoreceptor matrix and other regions of the retina.[45−48] Furthermore, differences in the glycosylation position between CNGA1 and CNGA3 observed in mammals may facilitate divergent sensitivities to MMPs for rod and cone photoreceptors. As a caveat, species- and tissue-specific features in protein glycosylation may complicate extrapolation from heterologous expression systems to photoreceptors. It is noteworthy, however, that the relative abundance of protected channels we observed with native rod photoreceptors (from *Xenopus*) was comparable to that of recombinant channels formed by $CNGA1_{NDN\text{-}TNS}$ subunits (see Figure 6C).

Removal of CNGA3 glycosylation by the N339Q mutation enhanced the susceptibility of CNG channels to MMP-dependent processing. This observation is relevant, as a variety of pathological conditions are associated with abnormal hypoglycosylation of protein substrates. Two prominent examples are the family of genetic diseases collectively termed congenital disorders of glycosylation (CDG)[49] and Chagas disease (caused by the flagellate protozoan *Trypanosoma cruzi*).[50] These conditions are often accompanied by cardiac conduction anomalies and arrhythmias, which have been linked to the glycosylation state of Na_V channels of the heart sarcolemma.[51] It is currently unknown whether an increased level of exposure of Na_V channels to extracellular proteases is a contributing factor in these disturbances. Furthermore, disorders of hypoglycosylation are associated with visual dysfunction. For example, both phosphomannomutase deficiency (PMM2-CDG) and dehydrodolichyl diphosphate synthase (DHDDS-CDG) have been causally linked to retinitis pigmentosa (RP).[52,53] Although it is suspected that CDG-associated RP is due, in part, to N-linked glycosylation deficiency in photoreceptors,[53] it is not understood how the attendant hypoglycosylation of protein substrates relates to the photoreceptor degeneration underlying RP. Increased Ca^{2+} influx through hyperactive CNG channels, resulting in photoreceptor cytotoxicity, is thought to be antecedent to several RP variants.[54−56] Considering that MMPs promote increased ligand sensitivity of CNG channels, and that MMP levels are increased in several retinal pathologies,[57−60] including an animal model of RP,[61] we speculate that enhanced MMP-dependent proteolysis of hypoglycosylated CNG channels may contribute to the pathophysiology of CDG-associated RP. Future studies will aim to explore the importance of CNGA glycosylation for photoreceptor function and the potential connection between CDG-associated RP- and MMP-dependent processing of CNG channels.

AUTHOR INFORMATION

Corresponding Author

*Department of Integrative Physiology and Neuroscience, Washington State University, P.O. Box 647620, Pullman, WA

99164. E-mail: varnum@wsu.edu. Telephone: (509) 335-0661. Fax: (509) 335-4650.

Funding

This work was supported by National Eye Institute Grants EY12836 to M.D.V. and EY19907 to R.L.B.

Notes

The authors declare no competing financial interest.

■ ACKNOWLEDGMENTS

We are grateful to W. N. Zagotta for sharing bovine CNGA1, S. E. Gordon for providing the human CNGB1 construct, and K.-W. Yau for sharing the cDNA clone for human CNGA3.

■ ABBREVIATIONS

CNG, cyclic nucleotide-gated; MMP, matrix metalloproteinase; ECM, extracellular matrix; cGMP, cyclic guanosine monophosphate; cAMP, cyclic adenosine monophosphate.

■ REFERENCES

(1) Craven, K. B., and Zagotta, W. N. (2006) CNG and HCN Channels: Two Peas, One Pod. *Annu. Rev. Physiol. 68*, 375−401.

(2) Pifferi, S., Boccaccio, A., and Menini, A. (2006) Cyclic nucleotide-gated ion channels in sensory transduction. *FEBS Lett. 580*, 2853−2859.

(3) Bradley, J., Reisert, J., and Frings, S. (2005) Regulation of cyclic nucleotide-gated channels. *Curr. Opin. Neurobiol. 15*, 343−349.

(4) Molday, R. S. (1996) Calmodulin regulation of cyclic-nucleotide-gated channels. *Curr. Opin. Neurobiol. 6*, 445−452.

(5) Rebrik, T. I., Botchkina, I., Arshavsky, V. Y., Craft, C. M., and Korenbrot, J. I. (2012) CNG-Modulin: A Novel Ca-Dependent Modulator of Ligand Sensitivity in Cone Photoreceptor cGMP-Gated Ion Channels. *J. Neurosci. 32*, 3142−3153.

(6) Molokanova, E., Trivedi, B., Savchenko, A., and Kramer, R. H. (1997) Modulation of rod photoreceptor cyclic nucleotide-gated channels by tyrosine phosphorylation. *J. Neurosci. 17*, 9068−9076.

(7) Gordon, S. E., Brautigan, D. L., and Zimmerman, A. L. (1992) Protein phosphatases modulate the apparent agonist affinity of the light-regulated ion channel in retinal rods. *Neuron 9*, 739−748.

(8) Müller, F., Vantler, M., Weitz, D., Eismann, E., Zoche, M., Koch, K.-W., and Kaupp, U. B. (2001) Ligand sensitivity of the α2 subunit from the bovine cone cGMP-gated channel is modulated by protein kinase C but not by calmodulin. *J. Physiol. 532*, 399−409.

(9) Womack, K. B., Gordon, S. E., He, F., Wensel, T. G., Lu, C. C., and Hilgemann, D. W. (2000) Do phosphatidylinositides modulate vertebrate phototransduction? *J. Neurosci. 20*, 2792−2799.

(10) Brady, J. D., Rich, E. D., Martens, J. R., Karpen, J. W., Varnum, M. D., and Brown, R. L. (2006) Interplay between PIP3 and calmodulin regulation of olfactory cyclic nucleotide-gated channels. *Proc. Natl. Acad. Sci. U.S.A. 103*, 15635−15640.

(11) Bright, S. R., Rich, E. D., and Varnum, M. D. (2007) Regulation of human cone cyclic nucleotide-gated channels by endogenous phospholipids and exogenously applied phosphatidylinositol 3,4,5-trisphosphate. *Mol. Pharmacol. 71*, 176−183.

(12) Dai, G., Peng, C., Liu, C., and Varnum, M. D. (2013) Two structural components in CNGA3 support regulation of cone CNG channels by phosphoinositides. *J. Gen. Physiol. 141*, 413−430.

(13) Korenbrot, J. I. (2012) Speed, adaptation, and stability of the response to light in cone photoreceptors: The functional role of Ca-dependent modulation of ligand sensitivity in cGMP-gated ion channels. *J. Gen. Physiol. 139*, 31−56.

(14) Ko, G. Y.-P., Ko, M. L., and Dryer, S. E. (2003) Circadian Phase-Dependent Modulation of cGMP-Gated Channels of Cone Photoreceptors by Dopamine and D2 Agonist. *J. Neurosci. 23*, 3145−3153.

(15) Ko, G. Y.-P., Ko, M. L., and Dryer, S. E. (2001) Circadian Regulation of cGMP-Gated Cationic Channels of Chick Retinal Cones. *Neuron 29*, 255−266.

(16) Meighan, P. C., Meighan, S. E., Rich, E. D., Brown, R. L., and Varnum, M. D. (2012) Matrix metalloproteinase-9 and -2 enhance the ligand sensitivity of photoreceptor cyclic nucleotide-gated channels. *Channels 6*, 181−196.

(17) Varki, A. (1993) Biological roles of oligosaccharides: All of the theories are correct. *Glycobiology 3*, 97−130.

(18) Spiro, R. G. (2002) Protein glycosylation: Nature, distribution, enzymatic formation, and disease implications of glycopeptide bonds. *Glycobiology 12*, 43R−56R.

(19) Lis, H., and Sharon, N. (1993) Protein glycosylation. Structural and functional aspects. *Eur. J. Biochem. 218*, 1−27.

(20) Much, B., Wahl-Schott, C., Zong, X., Schneider, A., Baumann, L., Moosmang, S., Ludwig, A., and Biel, M. (2003) Role of subunit heteromerization and N-linked glycosylation in the formation of functional hyperpolarization-activated cyclic nucleotide-gated channels. *J. Biol. Chem. 278*, 43781−43786.

(21) Wirkner, K., Hognestad, H., Jahnel, R., Hucho, F., and Illes, P. (2005) Characterization of rat transient receptor potential vanilloid 1 receptors lacking the N-glycosylation site N604. *NeuroReport 16*, 997−1001.

(22) Schwalbe, R. A., Wang, Z., Wible, B. A., and Brown, A. M. (1995) Potassium Channel Structure and Function as Reported by a Single Glycosylation Sequon. *J. Biol. Chem. 270*, 15336−15340.

(23) Rho, S., Lee, H. M., Lee, K., and Park, C. (2000) Effects of mutation at a conserved N-glycosylation site in the bovine retinal cyclic nucleotide-gated ion channel. *FEBS Lett. 478*, 246−252.

(24) Faillace, M. P., Bernabeu, R. O., and Korenbrot, J. I. (2004) Cellular Processing of Cone Photoreceptor Cyclic GMP-gated Ion Channels. *J. Biol. Chem. 279*, 22643−22653.

(25) Yu, W.-P., Grunwald, M. E., and Yau, K.-W. (1996) Molecular cloning, functional expression and chromosomal localization of a human homolog of the cyclic nucleotide-gated ion channel of retinal cone photoreceptors. *FEBS Lett. 393*, 211−215.

(26) Peng, C., Rich, E. D., and Varnum, M. D. (2004) Subunit configuration of heteromeric cone cyclic nucleotide-gated channels. *Neuron 42*, 401−410.

(27) Peng, C., Rich, E. D., Thor, C. A., and Varnum, M. D. (2003) Functionally important calmodulin-binding sites in both NH_2- and COOH-terminal regions of the cone photoreceptor cyclic nucleotide-gated channel CNGB3 subunit. *J. Biol. Chem. 278*, 24617−24623.

(28) Schoenmakers, T. J., Visser, G. J., Flik, G., and Theuvenet, A. P. (1992) CHELATOR: An improved method for computing metal ion concentrations in physiological solutions. *BioTechniques 12*, 870−874 , 876−879.

(29) Kusch, J., Zimmer, T., Holschuh, J., Biskup, C., Schulz, E., Nache, V., and Benndorf, K. (2010) Role of the S4-S5 linker in CNG channel activation. *Biophys. J. 99*, 2488−2496.

(30) Holm, S. (1979) A simple sequentially rejective multiple test proceedure. *Scandinavian Journal of Statistics 6*, 65−70.

(31) Okada, Y., Nagase, H., and Harris, E. D., Jr. (1986) A metalloproteinase from human rheumatoid synovial fibroblasts that digests connective tissue matrix components. Purification and characterization. *J. Biol. Chem. 261*, 14245−14255.

(32) Loh, Y. P., and Gainer, H. (1980) Evidence that glycosylation of pro-opiocortin and ACTH influences their proteolysis by trypsin and blood proteases. *Mol. Cell. Endocrinol. 20*, 35−44.

(33) Zhu, B. C., Fisher, S. F., Pande, H., Calaycay, J., Shively, J. E., and Laine, R. A. (1984) Human Placental (fetal) Fibronectin: Increased Glycosylation and Higher Protease Resistance Than Plasma Fibronectin. Presence of Polylactosamine Glycopeptides and Properties of a 44-Kilodalton Chymotryptic Collagen-Binding Domain: Difference from Human Plasma Fibronectin. *J. Biol. Chem. 259*, 3962−3970.

(34) Olden, K., Pratt, R. M., and Yamada, K. M. (1979) Role of carbohydrate in biological function of the adhesive glycoprotein fibronectin. *Proc. Natl. Acad. Sci. U.S.A. 76*, 3343−3347.

(35) Kasbaoui, L., Harb, J., Bernard, S., and Meflah, K. (1989) Differences in glycosylation state of fibronectin from two rat colon carcinoma cell lines in relation to tumoral progressiveness. *Cancer Res. 49*, 5317−5322.
(36) Tian, L., Stefanidakis, M., Ning, L., Van Lint, P., Nyman-Huttunen, H., Libert, C., Itohara, S., Mishina, M., Rauvala, H., and Gahmberg, C. G. (2007) Activation of NMDA receptors promotes dendritic spine development through MMP-mediated ICAM-5 cleavage. *J. Cell Biol. 178*, 687−700.
(37) Michaluk, P., Mikasova, L., Groc, L., Frischknecht, R., Choquet, D., and Kaczmarek, L. (2009) Matrix metalloproteinase-9 controls NMDA receptor surface diffusion through integrin beta1 signaling. *J. Neurosci. 29*, 6007−6012.
(38) Pugh, E. N., Jr., and Lamb, T. D. (1993) Amplification and kinetics of the activation steps in phototransduction. *Biochim. Biophys. Acta 1141*, 111−149.
(39) Ruiz, M., Brown, R. L., He, Y., Haley, T. L., and Karpen, J. W. (1999) The single-channel dose-response relation is consistently steep for rod cyclic nucleotide-gated channels: Implications for the interpretation of macroscopic dose-response relations. *Biochemistry 38*, 10642−10648.
(40) Chow, J. P. H., Fujikawa, A., Shimizu, H., Suzuki, R., and Noda, M. (2008) Metalloproteinase- and γ-secretase-mediated cleavage of protein-tyrosine phosphatase receptor type Z. *J. Biol. Chem. 283*, 30879−30889.
(41) Hayashi, H., and Yamashita, Y. (2012) Role of N-glycosylation in cell surface expression and protection against proteolysis of the intestinal anion exchanger SLC26A3. *Am. J. Physiol. 302*, C781−C795.
(42) Gahring, L., Carlson, N. G., Meyer, E. L., and Rogers, S. W. (2001) Granzyme B proteolysis of a neuronal glutamate receptor generates an autoantigen and is modulated by glycosylation. *J. Immunol. 166*, 1433−1438.
(43) Mellquist, J. L., Kasturi, L., Spitalnik, S. L., and Shakin-Eshleman, S. H. (1998) The Amino Acid Following an Asn-X-Ser/Thr Sequon Is an Important Determinant of N-Linked Core Glycosylation Efficiency. *Biochemistry 37*, 6833−6837.
(44) Cohen, D. M. (2006) Regulation of TRP channels by N-linked glycosylation. *Semin. Cell Dev. Biol. 17*, 630−637.
(45) Plantner, J. J., and Drew, T. A. (1994) Polarized distribution of metalloproteinases in the bovine interphotoreceptor matrix. *Exp. Eye Res. 59*, 577−585.
(46) Padgett, L. C., Lui, G. M., Werb, Z., and LaVail, M. M. (1997) Matrix metalloproteinase-2 and tissue inhibitor of metalloproteinase-1 in the retinal pigment epithelium and interphotoreceptor matrix: Vectorial secretion and regulation. *Exp. Eye Res. 64*, 927−938.
(47) Smine, A., and Plantner, J. J. (1997) Membrane type-1 matrix metalloproteinase in human ocular tissues. *Curr. Eye Res. 16*, 925−929.
(48) Plantner, J. J., Smine, A., and Quinn, T. A. (1998) Matrix metalloproteinases and metalloproteinase inhibitors in human interphotoreceptor matrix and vitreous. *Curr. Eye Res. 17*, 132−140.
(49) Jaeken, J. (2010) Congenital disorders of glycosylation. *Ann. N.Y. Acad. Sci. 1214*, 190−198.
(50) Libby, P., Alroy, J., and Pereira, M. E. (1986) A neuraminidase from *Trypanosoma cruzi* removes sialic acid from the surface of mammalian myocardial and endothelial cells. *J. Clin. Invest. 77*, 127−135.
(51) Montpetit, M. L., Stocker, P. J., Schwetz, T. A., Harper, J. M., Norring, S. A., Schaffer, L., North, S. J., Jang-Lee, J., Gilmartin, T., Head, S. R., Haslam, S. M., Dell, A., Marth, J. D., and Bennett, E. S. (2009) Regulated and aberrant glycosylation modulate cardiac electrical signaling. *Proc. Natl. Acad. Sci. U.S.A. 106*, 16517−16522.
(52) Jensen, H., Kjaergaard, S., Klie, F., and Moller, H. U. (2003) Ophthalmic manifestations of congenital disorder of glycosylation type 1a. *Ophthalmic Genet. 24*, 81−88.
(53) Züchner, S., Dallman, J., Wen, R., Beecham, G., Naj, A., Farooq, A., Kohli, M. A., Whitehead, P. L., Hulme, W., Konidari, I., Edwards, Y. J. K., Cai, G., Peter, I., Seo, D., Buxbaum, J. D., Haines, J. L., Blanton, S., Young, J., Alfonso, E., Vance, J. M., Lam, B. L., and Peričak-Vance, M. A. (2011) Whole-Exome Sequencing Links a Variant in DHDDS to Retinitis Pigmentosa. *Am. J. Hum. Genet. 88*, 201−206.
(54) Koch, S., Sothilingam, V., Garcia Garrido, M., Tanimoto, N., Becirovic, E., Koch, F., Seide, C., Beck, S. C., Seeliger, M. W., Biel, M., Mühlfriedel, R., and Michalakis, S. (2012) Gene therapy restores vision and delays degeneration in the CNGB1$^{(-/-)}$ mouse model of retinitis pigmentosa. *Hum. Mol. Genet. 21*, 4486−4496.
(55) Paquet-Durand, F., Beck, S., Michalakis, S., Goldmann, T., Huber, G., Mühlfriedel, R., Trifunović, D., Fischer, M. D., Fahl, E., Duetsch, G., Becirovic, E., Wolfrum, U., van Veen, T., Biel, M., Tanimoto, N., and Seeliger, M. W. (2011) A key role for cyclic nucleotide gated (CNG) channels in cGMP-related retinitis pigmentosa. *Hum. Mol. Genet. 20*, 941−947.
(56) Tosi, J., Davis, R. J., Wang, N.-K., Naumann, M., Lin, C.-S., and Tsang, S. H. (2011) shRNA knockdown of guanylate cyclase 2e or cyclic nucleotide gated channel α1 increases photoreceptor survival in a cGMP phosphodiesterase mouse model of retinitis pigmentosa. *J. Cell. Mol. Med. 15*, 1778−1787.
(57) Plantner, J. J., Jiang, C., and Smine, A. (1998) Increase in interphotoreceptor matrix gelatinase A (MMP-2) associated with age-related macular degeneration. *Exp. Eye Res. 67*, 637−645.
(58) Chen, Y. D., Xu, X., Xia, X., Wu, H., Liu, K., Zheng, Z., and Zhu, D. (2008) MMP9 is involved in glycation end-products induced increase of retinal vascular permeability in rats and the therapeutic effect of minocycline. *Curr. Eye Res. 33*, 977−983.
(59) Zhang, X., Cheng, M., and Chintala, S. K. (2004) Kainic acid-mediated upregulation of matrix metalloproteinase-9 promotes retinal degeneration. *Invest. Ophthalmol. Visual Sci. 45*, 2374−2383.
(60) Mali, R. S., Cheng, M., and Chintala, S. K. (2005) Intravitreous injection of a membrane depolarization agent causes retinal degeneration via matrix metalloproteinase-9. *Invest. Ophthalmol. Visual Sci. 46*, 2125−2132.
(61) Ahuja, S., Ahuja, P., Caffé, A. R., Ekstrom, P., Abrahamson, M., and van Veen, T. (2006) rd1 mouse retina shows imbalance in cellular distribution and levels of TIMP-1/MMP-9, TIMP-2/MMP-2 and sulfated glycosaminoglycans. *Ophthalmic Res. 38*, 125−136.
(62) Arnold, K., Bordoli, L., Kopp, J., and Schwede, T. (2006) The SWISS-MODEL workspace: A web-based environment for protein structure homology modelling. *Bioinformatics 22*, 195−201.
(63) Guex, N., and Peitsch, M. C. (1997) SWISS-MODEL and the Swiss-PdbViewer: An environment for comparative protein modeling. *Electrophoresis 18*, 2714−2723.
(64) Schwede, T., Kopp, J., Guex, N., and Peitsch, M. C. (2003) SWISS-MODEL: An automated protein homology-modeling server. *Nucleic Acids Res. 31*, 3381−3385.